

A comparative Analysis of Cylindrical CFS-PML ABC for Finite Volume Simulations in the Frequency Domain

Ana Paula M. Lima and Marcela S. Novo

Department of Electrical Engineering - Federal University of Bahia - Rua Aristides Novis, 2, Federação, Salvador-BA, Brasil, 40210-630. marcela.novo@ufba.br

Abstract— A comparative analysis of two cylindrical complex-frequency-shifted perfectly matched layers (CFS-PML) absorbing boundary condition (ABC) for bi-dimensional (2-D) finite-volume (FV) simulations in the frequency domain is presented. The impact of CFS-PML parameters on the wave absorption, as well as on the condition number of the associated system matrix is investigated by comparing the performance of two PML loss profiles, viz., polynomial and geometric grading. FV-CFS-PML results are validated against analytical solution. Numerical results show that inclusion of a CFS-PML within the FV computational domain increases the condition number of the system matrix and therefore the use of CFS-PML 3-D FV simulations is limited.

Index Terms— Coaxial waveguides, condition number, finite volume methods, perfectly matched layers.

I. INTRODUCTION

One of the biggest challenges in the computational electromagnetics modeling is the efficient and accurate solution of electromagnetic fields in unbounded problems. In the analysis of large scale problems, it is essential to employ iterative solvers for the resulting associated sparse linear system. In general, the convergence of these solvers becomes poorer as the condition number of the system matrix increases and, it may not be achieved in many cases. Furthermore, in order to simulate unbounded problems in both lossless and low-loss media, an absorbing boundary condition (ABC) must be constructed to eliminate spurious reflections from computational boundaries. The perfectly matched layers (PML) ABC has been shown to be very effective for discrete methods [1]–[5]. However, some papers in the literature report that the use of PML in frequency domain methods, such as the finite-volume and finite-element, increases the condition number and consequently, the solution can be plagued by convergence problems [6]–[8]. It should be note that the problem associated with the condition number is not really predicated on frequency domain methods but rather whether the method produces require the solution of a large system matrix or not. Time domain methods such as finite-volume time-domain (FVTD) and finite-element time-domain (FETD) do require such step and

can be also affected by the condition number [9]. On the other hand, some frequency domain methods such as the numerical mode matching (NMM) can produce much smaller matrices and be less affected by the condition number issue [10].

A three-dimensional (3-D) finite volume (FV) algorithm has been developed and successfully applied to simulate electromagnetic (EM) well-logging tool response in high-loss geophysical formations [11]–[14]. In low-loss media, however, its application implies increasing the computational domain. To save memory requirements and CPU time, a PML must be incorporated in the outermost cells of the grid in order to absorb outgoing waves.

The degradation of the condition number of FV system matrices after the implementation of the PMLs in the computational domain was first investigated in [15], where coaxial waveguides terminated by PMLs in the longitudinal direction were analyzed in terms of its loss parameters and number of layers. In [16], a similar study was done but with coaxial waveguides terminated by longitudinal complex-frequency-shifted (CFS) PMLs [17].

In this paper, a 2-D FV algorithm is applied to a coaxial waveguide backed by a cylindrical CFS-PML in both longitudinal and radial directions. This geometry mimics a FV computational domain with a metallic mandrel around the z axis, which is common in EM well-logging tools simulations. Here, the main objective is to analyze the effect of the CFS-PML parameters on the condition number of the FV system matrix taking also into account the numerical discretization error. We assess this by comparing the performance of two PML loss profiles, viz., polynomial and geometric grading. Furthermore, the numerical reflection coefficient is also investigated. The FV-CFS-PML technique is validated against analytical solution showing very good agreement. Numerical results show that the inclusion of a CFS-PML within the FV computational domain increases substantially the condition number of the system matrix. Therefore, unless a well-conditioned CFS-PML is developed, the use of CFS-PML 3-D FV simulations is limited since it requires the use of a direct method for solving the FV system matrix.

II. FORMULATION

A. Finite Volume Technique

In the FV technique, the physical space is decomposed into small volumes and the partial differential equations (PDE) are integrated over each volume. The present FV technique is based on a staggered-grid scheme developed in cylindrical coordinates to better conform to the majority of well-logging tool geometries and to avoid staircasing errors [18]. The computational grid is uniform in both the longitudinal z -direction and the radial ρ -direction. Ampere's law is integrated over faces of the dual grid $\tilde{\Omega}$. For any surface $\tilde{S} \subset \tilde{\Omega}$ with boundary $\partial\tilde{S}$, this gives ($e^{-i\omega t}$ convention):

$$\oint_{\partial\tilde{S}} \vec{H} \cdot d\vec{l} - \iint_{\tilde{S}} (\sigma - i\omega\epsilon) \vec{E} \cdot d\vec{s} = \iint_{\tilde{S}} \vec{J}_s \cdot d\vec{s} \tag{1}$$

where σ and ε are the conductivity, and permittivity of the medium, respectively. \vec{J}_s is the electric current density (impressed source). The electric and magnetic fields are the unknowns to be determined. Dirichlet boundary conditions are assumed at the computational boundaries. Discrete equations are obtained by evaluating the above over each face of the dual grid. By using integration dual faces \tilde{S} perpendicular to the ϕ -direction (Fig. 1a), we arrive at:

$$\frac{H_\rho(i, k + \frac{1}{2}) - H_\rho(i, k - \frac{1}{2})}{\Delta z} - \frac{H_z(i + \frac{1}{2}, k) - H_z(i - \frac{1}{2}, k)}{\Delta \rho} - \hat{\sigma}(i, k)E_\phi(i, k) = \frac{I_0(i, k)}{\Delta \rho \Delta z} \tag{2}$$

where i, k , refer to a primal grid nodal indexing, $\Delta \rho$ and Δz are the cylindrical grid spatial increments in the ρ - and z -directions, respectively; I_0 is the current source amplitude, and $\hat{\sigma} = (\sigma - i\omega\varepsilon)$. The magnetic field can be eliminated from (2) using Faraday's law:

$$\oint_{\partial S} \vec{E} \cdot d\vec{l} - \iint_S i\omega\mu\vec{H} \cdot d\vec{s} = 0 \tag{3}$$

where μ is the permeability of the medium.

By using integration primary faces S perpendicular to the ρ - and z -directions (Fig. 1b and Fig. 1c), we arrive at:

$$H_\rho(i, k + \frac{1}{2}) = \frac{1}{i\omega\mu\Delta z} [E_\phi(i, k) - E_\phi(i, k + 1)] \tag{4a}$$

$$H_z(i + \frac{1}{2}, k) = \frac{2}{i\omega\mu\Delta \rho} [\rho_{i+1}E_\phi(i + 1, k) - \rho_iE_\phi(i, k)] \tag{4b}$$

Substituting (4a) and (4b) into (2), a discrete linear system $[A][X]=[B]$ is obtained, where $[A]$ is a complex non-Hermitian matrix, $[X]$ is the vector of (electric field) degrees of freedom (DoFs), and $[B]$ is the discrete source representation.

B. Cylindrical Perfectly Matched Layers

A cylindrical PML is incorporated in the outermost cells of the grid in order to absorb outgoing waves. This is done by modifying the constitutive parameters inside the PML region, and hence it does not require any modification on Maxwell's equation themselves. In cylindrical coordinates, the PML constitutive tensors that are matched to a homogeneous nondispersive medium characterized by constitutive parameters ε and μ , are given by

$$\bar{\varepsilon}_{PML} = \varepsilon \bar{\Lambda}_{(\rho, \phi, z)}(\rho, z; \omega) ; \bar{\mu}_{PML} = \mu \bar{\Lambda}_{(\rho, \phi, z)}(\rho, z; \omega) \tag{5}$$

with [19]

$$\bar{\Lambda}_{(\rho, \phi, z)}(\rho, z; \omega) = \frac{\tilde{\rho}^{s_z}}{\rho^{s_\rho}} \hat{\rho} + \frac{\rho^{s_z} s_\rho}{\tilde{\rho}} \hat{\phi} + \frac{\tilde{\rho}^{s_\rho}}{\rho^{s_z}} \hat{z} \tag{6}$$

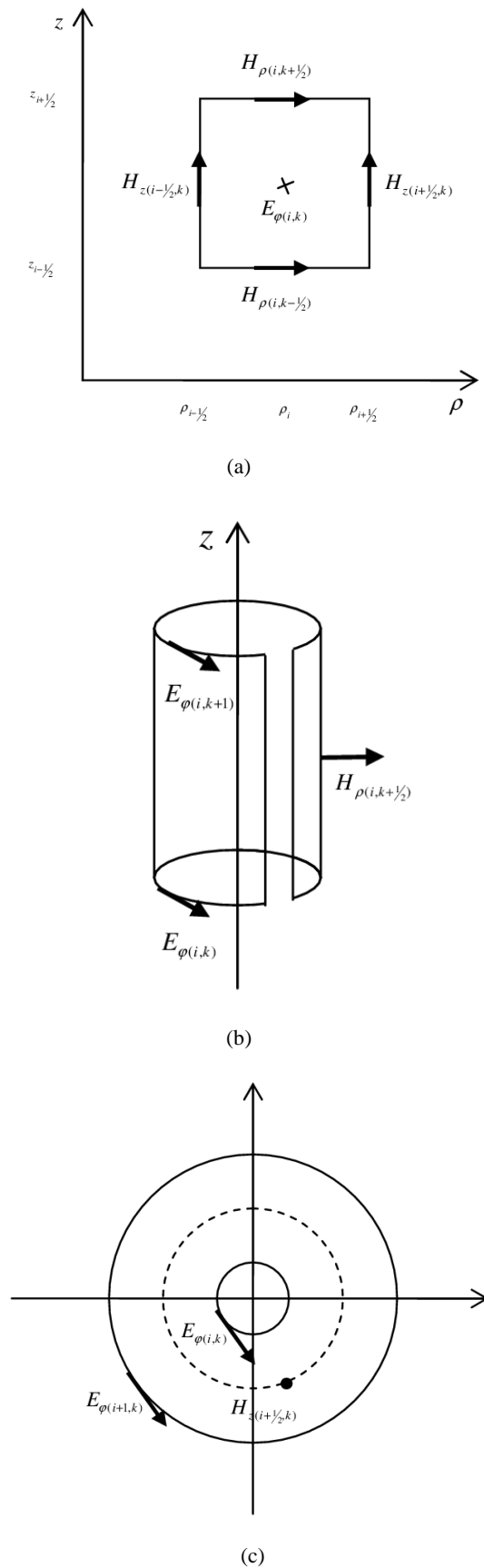


Fig. 1. Unit cell of the staggered grid scheme for spatial discretization of electromagnetic fields on the cylindrical grid. (a) Dual faces perpendicular to the ϕ - direction. (b) Primary faces perpendicular to the ρ - direction. (c) Primary faces perpendicular to the z - direction.

In the above, $\tilde{\rho}$ is the analytic continuation of the radial coordinate to a complex variable domain, and s_ρ and s_z are frequency-dependent complex stretching variables. Here, two types of PML are implemented for comparison purposes, viz., the standard PML and the CFS-PML. The stretching variables s_ρ and s_z are defined as:

$$s_\rho(\rho) = K_\rho(\rho) - \frac{\sigma_\rho(\rho)}{\alpha_\rho + i\omega\epsilon} ; s_z(z) = K_z(z) - \frac{\sigma_z(z)}{\alpha_z + i\omega\epsilon} \tag{7}$$

and

$$\tilde{\rho} = \int_0^\rho s_\rho(\rho') d\rho' \tag{8}$$

where $K_\rho(\rho)$, $\sigma_\rho(\rho)$, $K_z(z)$ and $\sigma_z(z)$ are functions of position only [11]. Note that in the standard PML the parameters α_ρ and α_z are set equal to zero.

Inside the CFS-PML region, ordinary longitudinal outgoing eigenmodes are transformed to $e^{-i\alpha_\zeta\beta|\zeta|} e^{-\beta \frac{\sigma_\zeta}{\alpha_\zeta + i\omega\epsilon} |\zeta|}$, where $\beta = \omega\sqrt{\mu\epsilon}$ and ζ stands for ρ or z ; and similarly for radial eigenfunctions in terms of Hankel functions. Hence, the transformed eigenmodes exhibit exponential decay inside the CFS-PML so as to reduce spurious reflections from the grid terminations. However, in the low-frequency limit $\omega \rightarrow 0$, the behavior does not exhibit induced attenuation. To circumvent this, is scaled to be maximum at the inner CFS-PML interface, and minimum at the grid termination. Here, the following scaling is adopted:

$$\alpha_\zeta(\zeta) = \alpha_\zeta^{\max} \left[1 - \left(\frac{\zeta}{d} \right)^m \right] \tag{9}$$

where d is the CFS-PML thickness and m is a taper profile for both real and imaginary parts of the stretching variables.

Once, the design of an effective CFS-PML requires balancing the theoretical reflection error, and the numerical discretization error; several profiles have been suggested for grading σ_ζ in the context of CFS-PML. The most successful use a polynomial or geometric variation of the CFS-PML loss. Here, the following polynomial and geometric grading are adopted [1].

1) Polynomial:

$$\sigma_\zeta(\zeta) = \left(\frac{\zeta}{d} \right)^m \sigma_\zeta^{\max} \tag{10a}$$

$$\sigma_\zeta^{\max} = - \frac{(m+1) \ln[R(\theta=0)]}{2\eta d} \tag{10b}$$

σ_ζ^{\max} is the CFS-PML conductivity at the outer boundary, θ is the incidence angle over CFS-PML, and $R(\theta)$ is the theoretical reflection error given by

$$R(\theta) = e^{-2\eta \cos(\theta) \int_0^d \sigma_\zeta(\zeta) d\zeta} \tag{10c}$$

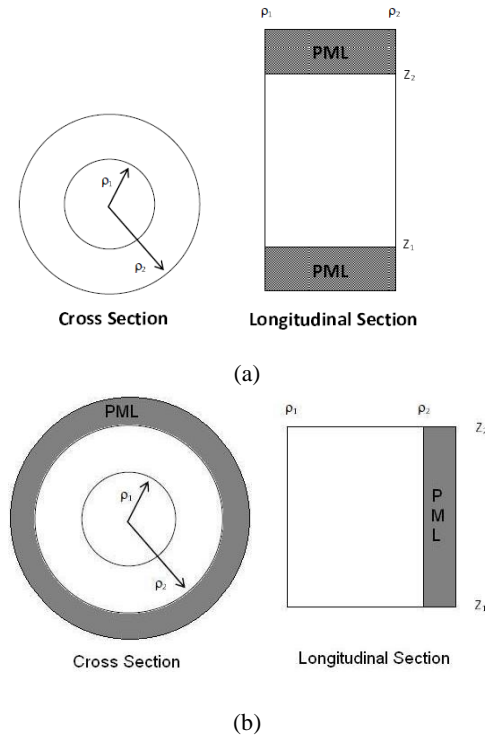


Fig. 2. Illustration of the geometry problem. (a) Longitudinal PML - (b) Radial PML

2) Geometric:

$$\sigma_{\zeta}(\zeta) = \left(g \frac{1}{\Delta_{\zeta}} \right)^{\zeta} \sigma_{\zeta}^0 \tag{11a}$$

$$\sigma_{\zeta}^0 = - \frac{\ln[R(\theta=0)] \ln(g)}{2\eta \Delta_{\zeta} \left(g^{\frac{d}{\Delta_{\zeta}}} - 1 \right)} \tag{11b}$$

where σ_{ζ}^0 is the CFS-PML conductivity at its surface, g is the scaling factor, and Δ_{ζ} is the FV space increment.

III. NUMERICAL RESULTS

A. Validation

In order to validate the present FV-CFS-PML method, the algorithm is applied to a lossless coaxial waveguide backed by a cylindrical CFS-PML in both the longitudinal and radial directions, as illustrated in Fig. 2(a) e 2(b), respectively. In all simulations performed here, unless mentioned otherwise, the

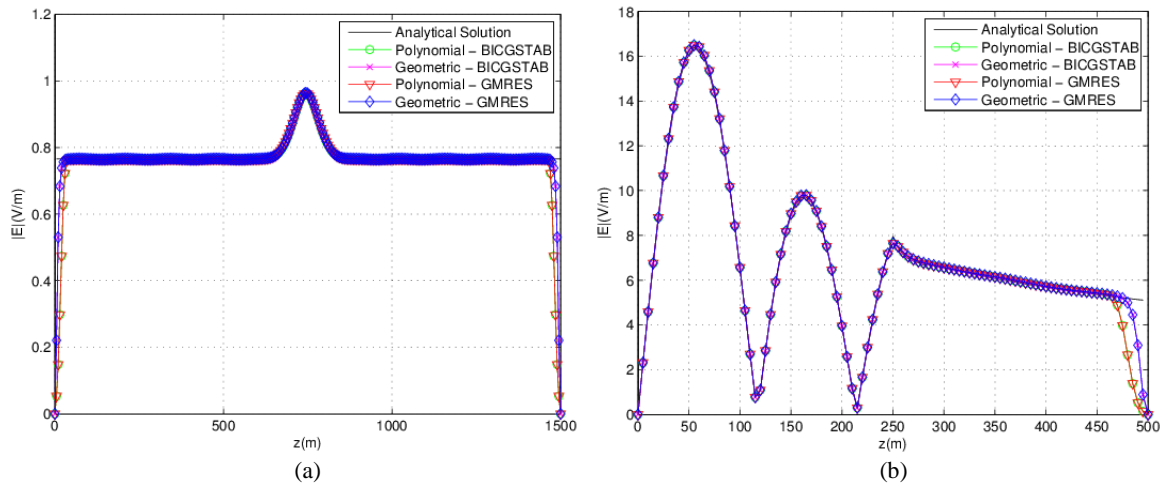


Fig. 3. Electric field distribution of a lossless coaxial waveguide backed by a cylindrical CFS-PML. (a) Longitudinal PML - (b) Radial PML

following input data are used: the operating frequency is 2 MHz; both the relative electric permittivity and magnetic permeability are set equal to 1; the inner cylinder has radius equal to $r = 0.1016$ m; the CFS-PML are set up using eight cells; $\alpha_{\zeta}^{\max} = 10^{-4}$ and the scaling factors are $m=2$ and $g=3.2$. For the longitudinal PML case, the computational domain is discretized using a $(N_{\rho}, N_z) = (50, 300)$ grid.

The discretization cell size is uniform in both directions with $\Delta_{\rho} = 2.2$ m and $\Delta_z = 5.0$ m. The source is set at $(N_{\rho}, N_z) = (10, 150)$ and the field is sampled at $\rho = 85.1$ m. For the radial PML case, a $(N_{\rho}, N_z) = (100, 80)$ grid is used. The discretization cell size is uniform in both directions with $\Delta_{\rho} = 5.0$ m and $\Delta_z = 1.5$ m. The source is set at $(N_{\rho}, N_z) = (51, 35)$ and the field is sampled at $\rho = 60.0$ m.

In fig. 3, the electric field distribution from the FV-PML simulation is compared against an analytical solution. Very good agreement is observed between the FV-PML and analytical results. This occurs because α_{ζ}^{\max} is selected within the range defined by $\alpha_{\zeta}^{\max} \leq \omega \epsilon_0$. Outside this range, the CFS-PML does not exhibit induced attenuation.

To better analyze the performance of the polynomial and geometric CFS-PML loss profiles, the numerical (actual) coefficient reflection (COEFN) as a function of the theoretical coefficient reflection (COEF) is plotted in Fig. 4, for different values of α_{ζ}^{\max} . For the longitudinal CFS-PML case, it can be noted that the polynomial-graded profile provides smaller reflection levels, showing an advantage over the geometric-graded profile. However, α_z^{\max} does not have strong influence on the reflection level in both profiles. On the other hand, the COEFN does not vary with α_{ρ}^{\max} in both profiles for radial CFS-PML. Moreover, polynomial and geometric profiles provide similar reflection levels. As expected, it can also be noted that for $\alpha_{\zeta}^{\max} \leq \omega \epsilon_0$, the CFS-PML does not offer additional

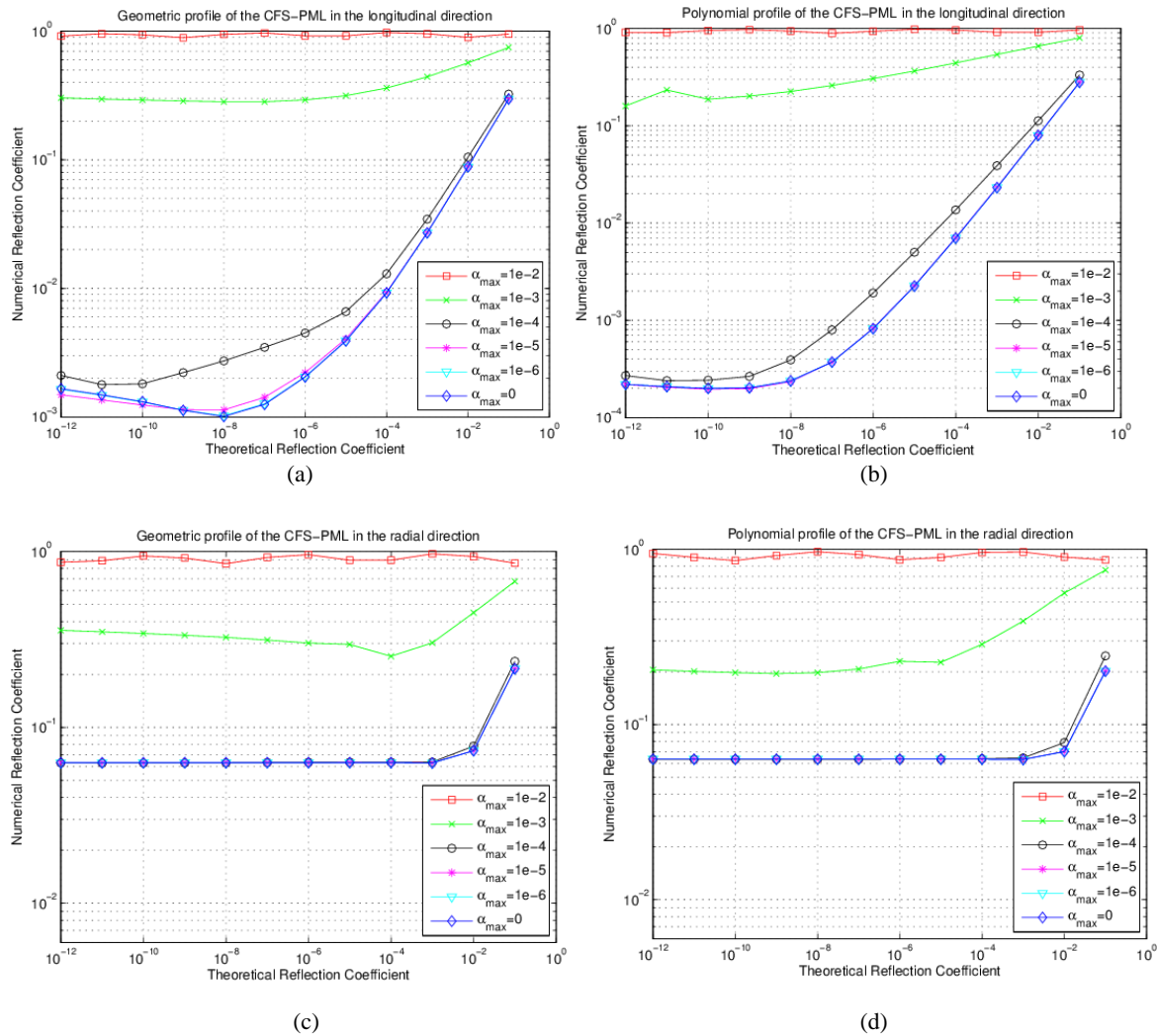


Fig. 4. Numerical Reflection Coefficient X Theoretical reflection coefficient for different values of α_z^{\max} . In both profiles, NPML=6 and KPML=1.

attenuation. It should be noted that the design of an effective CFS-PML requires balancing the theoretical reflection error and the numerical discretization error. Normally, the CFS-PML conductivity profile is chosen as large as possible to minimize the theoretical reflection error. Unfortunately, if the CFS-PML conductivity profile is too large, the discretization error due to the FV approximation dominates, and the numerical (actual) reflection error is potentially orders of magnitude higher than what equation (10c) predicts. This problem is more pronounced in our case because the cell size is too small.

Fig. 5 shows the COEFN as a function of α_z^{\max} for different values of KPML (the real part of the stretching variable s_z). For the longitudinal CFS-PML case, it is observed that both profiles show similar behavior, and the polynomial CFS-PML outperforms the geometric one. Note that for $\alpha_z^{\max} > 10^{-4}$, COEFN has considerably increased in both profiles and for $\alpha_z^{\max} \leq 10^{-4}$, a slight variation is observed in the geometric profile. However, for the radial CFS-PML case, it can be noted that COEFN does not vary neither with COEF nor with KPML in both profiles.

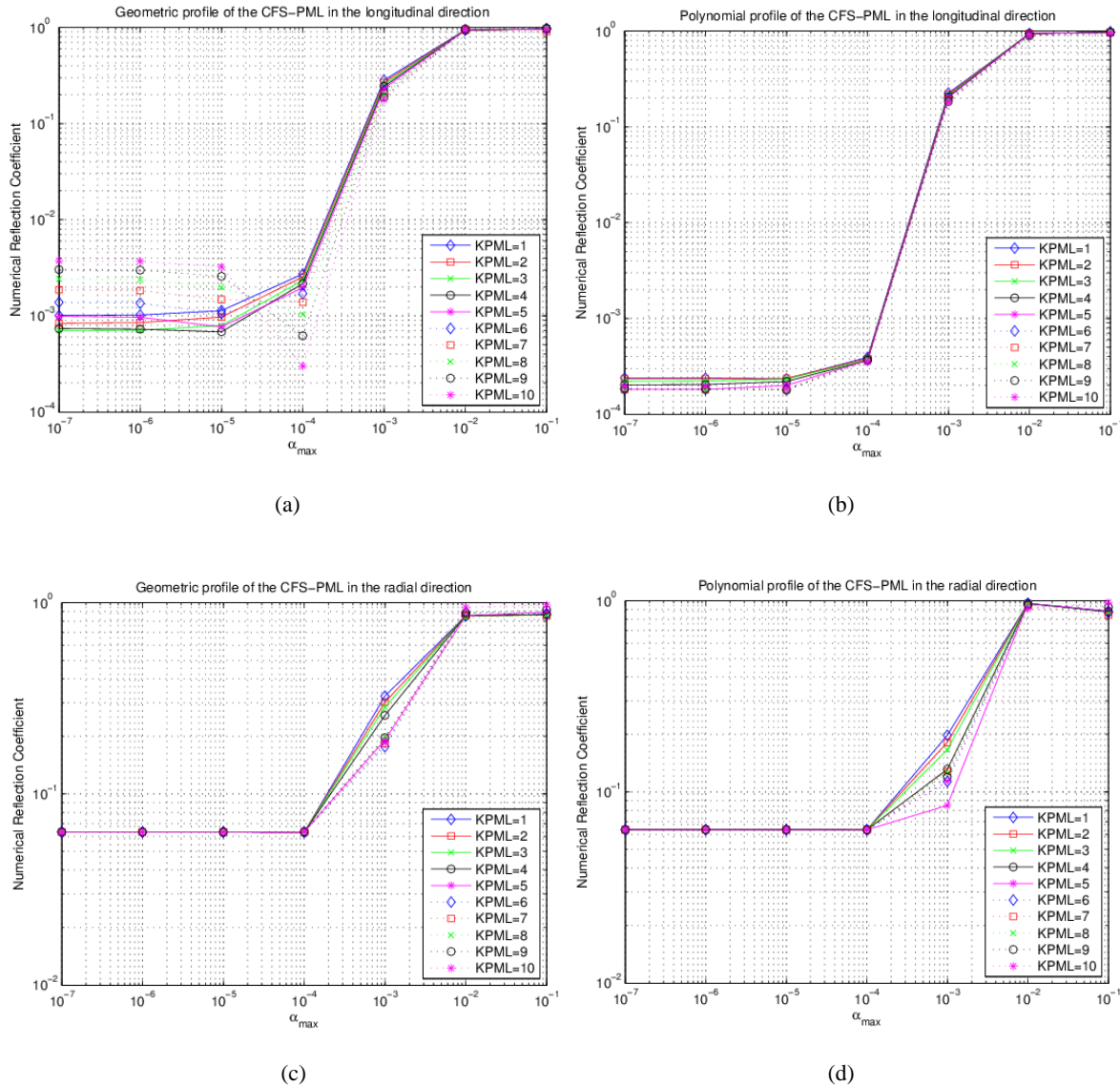


Fig. 5. Numerical Reflection Coefficient $\times \alpha_{\zeta}^{\max}$ for different values of KPML. In both profiles, NPML=6.

To investigate the impact of CFS-PML parameters on the condition number (CN) of the FV system matrix, some of the input data have their values modified. In this study, the computational domain is discretized using a $(N_{\rho}, N_z) = (50, 50)$ grid and the source is set at $(N_{\rho}, N_z) = (25, 25)$. The discretization cell size is uniform in both directions. For the longitudinal PML case, the domain was discretized by using $\Delta_{\rho} = 2.2m$ and $\Delta_z = 7.5m$; and for the radial PML case, $\Delta_{\rho} = 2.2m$ and $\Delta_z = 7.5m$ was used. Fig. 6 shows the CN as a function of COEF for different values of α_{ζ}^{\max} . For both the longitudinal and the radial CFS-PML case, it is observed that for $\alpha_{\zeta}^{\max} \leq 10^{-4}$ the CN decays as the COEF increases. Moreover, it can be noted that both profiles (polynomial and geometric) show similar behavior. Fig. 7 shows the CN as a function of α_{ζ}^{\max} for different values of KPML. Note that for $\alpha_{\zeta}^{\max} \leq 10^{-4}$, the KPML plays no role in the CN.

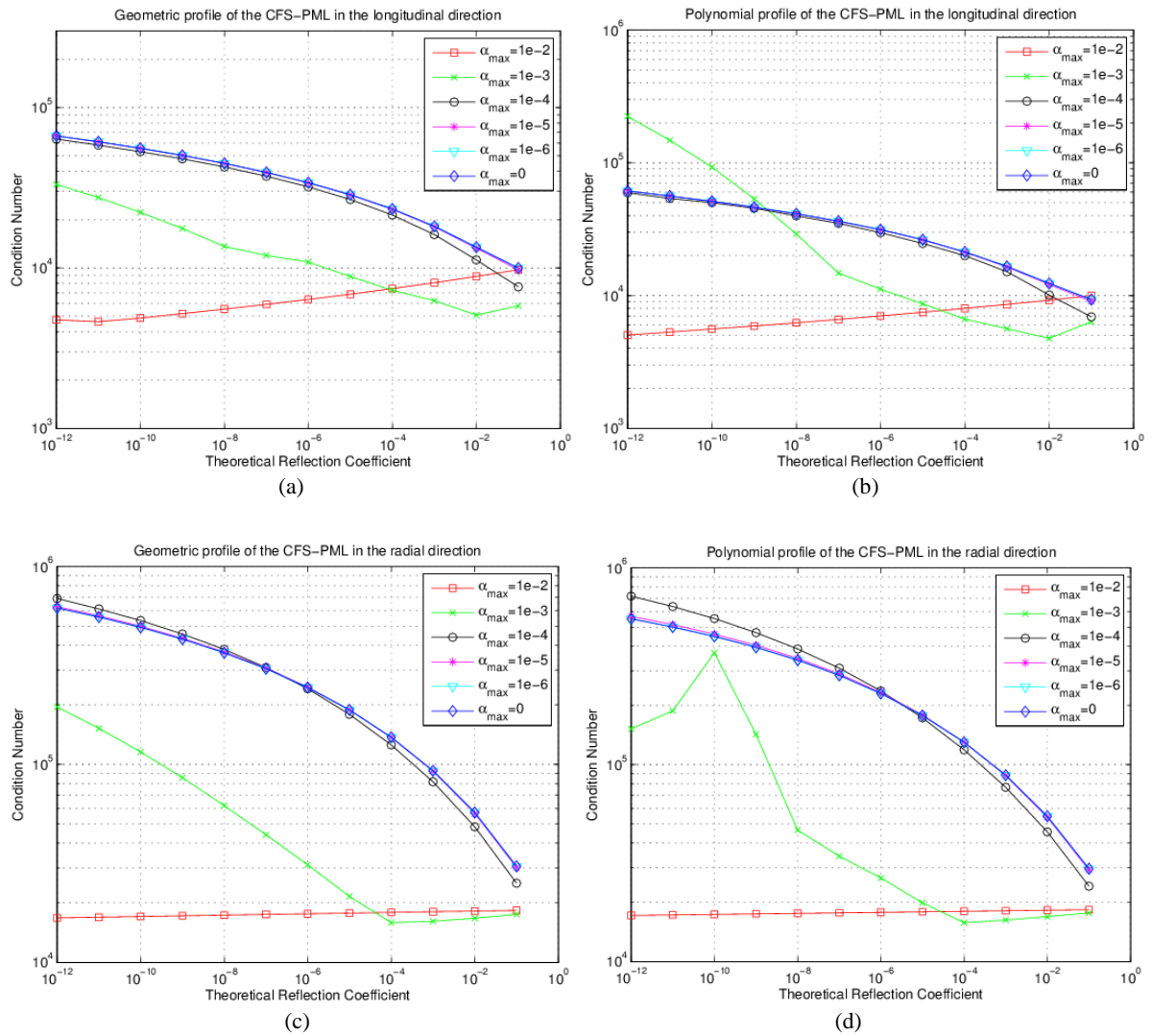


Fig. 6. Condition Number X Theoretical Reflection Coefficient for different values of α_{ζ}^{\max} . In both profiles, NPML=6 and KPML=1.

IV. CONCLUSION

We have compared the performance of two cylindrical CFS-PML, viz., polynomial-graded CFS-PML and geometric-graded CFS-PML for being used as an absorbing boundary condition (ABC) in the bi-dimensional (2-D) finite-volume technique in the frequency domain. Simulations in both the longitudinal and radial coaxial waveguide terminated by a cylindrical CFS-PML have been carried out. For the longitudinal CFS-PML case, the polynomial-graded CFS-PML has outperformed geometric-graded PML in terms of wave absorption. However, the condition number of the associated matrix system in both profiles are similar. For the radial CFS-PML case, both types of CFS-PML have shown similar performance in terms of absorption of the wave, as well as the condition number of the matrix system. Even though the CFS-PML has achieved great success in time-domain analysis, its usefulness in the frequency-domain methods remains unclear. The inclusion of the CFS-PML in

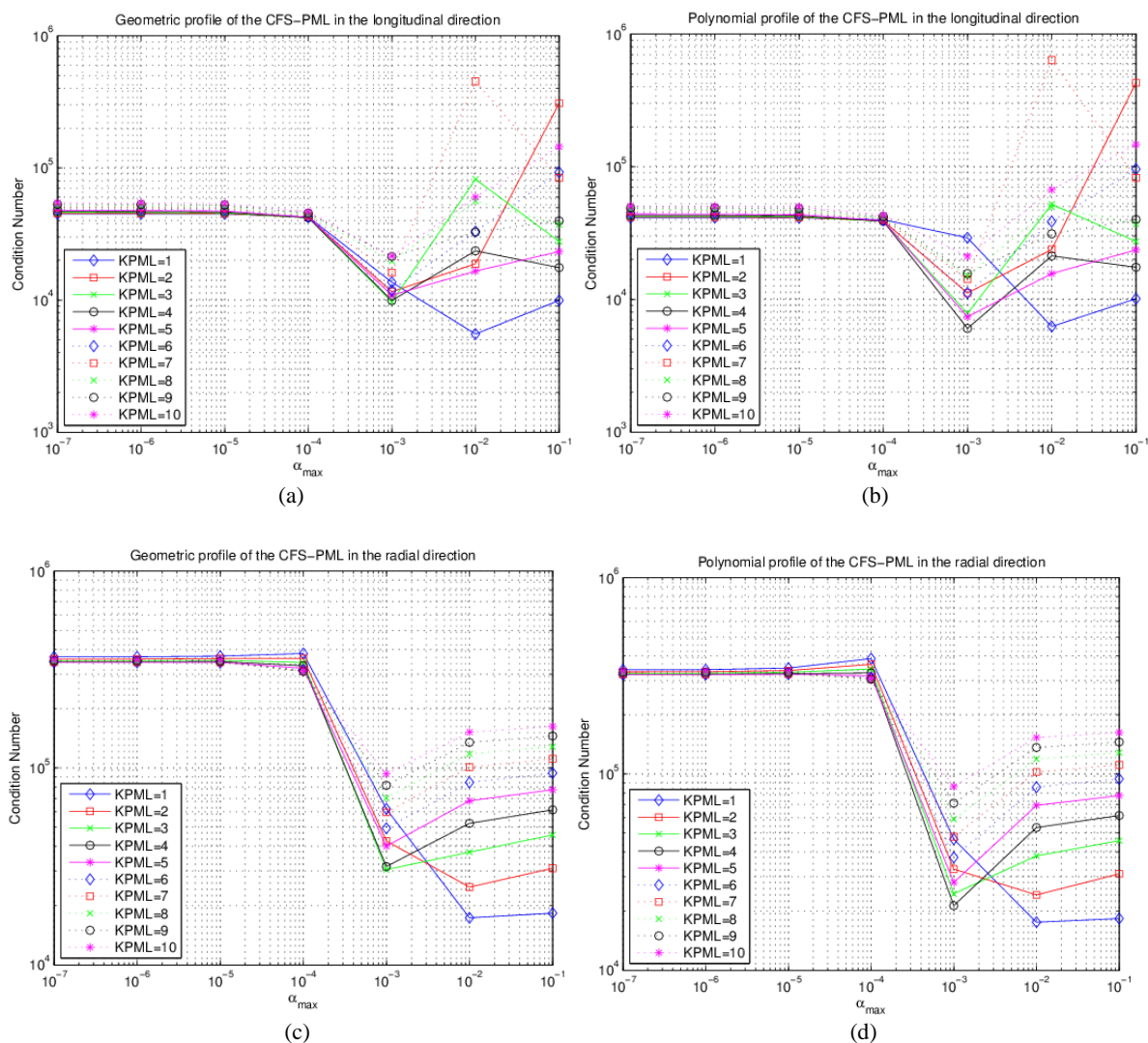


Fig. 7. Condition Number $\times \alpha_{\zeta}^{\max}$ for different values of KPML. In both profiles, NPML=6.

computational domain significantly increases the condition number of the system matrix and consequently the convergence of iterative methods deteriorates.

REFERENCES

- [1] A. Taflov and S. Hagness, *Computational Eletrodynamics: The Finite-Difference Time-Domain Method*, Boston MS: Artech House, 2005.
- [2] U. Pekel and R. Mittra, *A finite element method frequency-domain application of the perfectly matched layer (PML) concept*, *Microwave Opt. Technol. Lett.*, vol. 9, pp.117 -122, 1995.
- [3] Y. Y. Botros and J. L. Volakis, *Preconditioned generalized minimal residual iterative scheme for perfectly matched layer terminated applications*, *IEEE Micro. and Guide Wave Lett.*, vol. 9, no.2, Feb. 1999.
- [4] D. Pardo, L. Demkowicz, C. Torres-Verdin, and C. Michler, *PML Enhanced With A Self-Adaptive Goal-Oriented pp-Finite Element Method: Simulation Of Through-Casing Borehole Resistivity Measurements*, *Siam Journal on Scientific Computing*, vol 30, no. 6, pp. 2948-2964, 2008.
- [5] H. O. Lee, F. L. Teixeira, L. E. San Martin, and M. S. Bittar, *Numerical modeling of eccentered LWD borehole sensors in dipping and fully anisotropic Earth formations*, *IEEE Trans. Geosci. Remote Sens.*, vol. 50, no. 3, pp. 727-735, 2012.
- [6] J. M. Jin and W.C. Chew, *Combining PML and ABC for Finite Element Analysis of Scattering Problems*, *Micro. and Opt. Tech. Lett.*, vol. 12, no. 4, pp. 192-197, Jul. 1996.
- [7] Y. Y. Botros and J. L. Volakis, *Perfectly Matched Layer Termination for Finite-Element Meshes: Implementation and Application*, *Micro. and Opt. Tech. Lett.*, vol. 23, no. 7, pp. 166-172, Nov. 1999.

- [8] B. Stupfel, *A Study of the Condition Number of Various Finite Element Matrices Involved in the Numerical Solution of Maxwell's Equations*, IEEE Trans. Antennas Propag., vol. 52, no. 11, pp. 3048-3059, Nov. 2004.
- [9] E. S. Um, J. M. H. and D. L. Alumbaugh, *An iterative finite-element time-domain method for simulating three-dimensional electromagnetic diffusion in earth*, Geophysical Journal International, vol.190, no.2, pp. 871-886, Aug. 2012.
- [10] Y.K. Hue and F. L. Teixeira, *Numerical Mode-Matching Method for Tilted-Coil Antennas in Cylindrically Layered Anisotropic Media With Multiple Horizontal Beds*, IEEE Trans. Geoscience Remote Sens., vol.45, no.8, pp.2451-2462, 2007.
- [11] M. S. Novo, L. C. da Silva and F. L. Teixeira, *Finite Volume Modeling of Borehole Electromagnetic Logging in 3-D Anisotropic Formations Using Coupled Scalar-Vector potentials*, IEEE Antennas Wireless Propag. Lett., vol. 6, pp. 549-552, 2007.
- [12] M. S. Novo, L. C. da Silva and F. L. Teixeira, *Comparison of Coupled potentials and Field-Based Finite-Volume Techniques for Modeling of Borehole EM Tools*, IEEE Geosci. Remote Sens. Lett., vol. 5, pp. 209-211, 2008.
- [13] M. S. Novo, L. C. da Silva and F. L. Teixeira, *Three-Dimensional Finite-Volume Analysis of Directional Resistivity Logging Tools*, IEEE Trans. Geosci. Remote Sens., vol. 48, pp. 1151-1158, Mar. 2010.
- [14] M. S. Novo, L. C. da Silva and F. L. Teixeira, *A Comparative Analysis of Krylov Solvers for Three-Dimensional Simulations of Borehole Sensors*, IEEE Geosci. Remote Sens. Lett., vol. 8, no. 1, pp. 98-102, Jan. 2011.
- [15] L. F. Ribeiro and M. S. Novo, *Analysis of the Cylindrical PML ABC for 2-D Finite Volume Simulations in the Frequency Domain*, Proceedings of 2011 SBMO/IEEE MTT-S International Microwave and Optoelectronics Conference, 2011, Natal.
- [16] A. P. M. Lima and M. S. Novo, *Analysis of Cylindrical CFS-PML ABC for 2-D Finite Volume Simulations in the Frequency Domain*, Proceedings of of 2013 SBMO/IEEE MTT-S International Microwave and Optoelectronics Conference, 2013, Rio de Janeiro.
- [17] M. Kuzuoglu and R. Mittra, *"Frequency dependence of the constitutive parameters of causal perfectly matched absorbers,"* IEEE Microwave Guided Wave Lett., vol. 6, pp. 447-449, Dec. 1996.
- [18] M. S. Novo, *Análise numérica de sensores eletromagnéticos de prospecção petrolífera utilizando o método dos volumes finitos*, Pontifícia Universidade Católica do Rio de Janeiro, Departamento de Engenharia Elétrica, Tese de Doutorado, Agosto 2007.
- [19] F. L. Teixeira and W. C. Chew, *Systematic Derivation of Anisotropic PML Absorbing Media in Cylindrical and Spherical Coordinates*, IEEE Microwave Guided Wave Lett., vol. 7, no. 11, pp. 371-373, Nov. 1997.